catalysts

MDPI

Article

Application of Wolkenstein's Electronic Theory to Size Effects in CO Oxidation over ZnO Nanocatalysts

Gulnara Kosmambetova [1], Nigora Turaeva [2,*], Olga Didenko [1] and Peter Strizhak [1]

[1] Department of Heterogeneous Catalysis and Chemical Kinetics, L.V. Pisarzhevskii Institute of Physical Chemistry of the National Academy of Sciences of Ukraine, Prosp. Nauky, 31, 03028 Kyiv, Ukraine; kosmambetova@ukr.net (G.K.); o.z.didenko@gmail.com (O.D.); pstrizhak@hotmail.com (P.S.)

[2] Department of Natural Sciences and Mathematics, Webster University, 470 East Lockwood Avenue, St. Louis, MO 63119, USA

* Correspondence: nigoraturaeva82@webster.edu

Abstract

The volcano-shaped dependence of the catalytic activity of the magnesia-supported ZnO nanoparticles on their diameter in CO oxidation was considered in the framework of Wolkenstein's electron theory of catalysis on semiconductors. By analyzing the diffuse reflectance UV-Vis spectra of the ZnO nanoparticles in catalysts, we demonstrate that a narrow range of particle diameters (4.0–4.6 nm) leads to changes in the Fermi level due to quantum confinement of free electrons. As the diameter of the ZnO nanoparticles decreases, the Fermi level rises, resulting in an accelerated acceptor stage and a decelerated donor stage involving free electrons interacting with atomic oxygen and carbon dioxide on the catalyst surface, respectively. This opposing change in the rates of the donor and acceptor stages during the CO oxidation reaction, influenced by the diameter of the ZnO nanoparticles, gives rise to a volcano-shaped size dependence of the reaction rate. Furthermore, an optimal catalyst particle diameter is identified, at which the reaction rate reaches its maximum.

Keywords: catalyst; ZnO nanoparticles; CO oxidation; Wolkenstein's electronic theory; volcano-shaped size dependence

1. Introduction

A volcano-shaped correlation between the rate of a heterogeneous catalytic reaction and the energy characteristics of the reagents and the catalyst is a consequence of the Sabatier principle, the fundamental principle of heterogeneous catalysis. According to this principle, the optimal interaction, neither too strong nor too weak, of adsorbed molecules with the catalyst surface is achieved by balancing the heats of adsorption of reagents and desorption of reaction products [1]. The validity of this approach is confirmed by the appearance of a volcano-shaped dependence of the reaction rate on the particle size of the catalyst. This is generally observed for nanocatalysts with an active component size less than 10 nm, the catalytic activity of which is due to the manifestation of the electronic factor to a greater extent than the geometric one [2]. Based on kinetic analysis, it was shown that the Gibbs energy of the formation of an activated complex also depends on the number of atoms on the faces, edges and corners of a nanoparticle, i.e., on its size, and thus reflects the relation between the influence of geometric and electronic effects on catalytic activity [3,4]. The appearance of theoretical interpretations of volcano-shaped plots using the main energetic quantities in the fields of heterogeneous catalysis is partly due to the development of the density functional theory (DFT) computations. It is especially

Check for updates

Academic Editor: Carlos Omar Castillo Araiza

Received: 29 January 2026
Revised: 9 March 2026
Accepted: 12 March 2026
Published: 14 March 2026

Copyright: © 2026 by the authors. Licensee MDPI, Basel, Switzerland. This article is an open access article distributed under the terms and conditions of the Creative Commons Attribution (CC BY) license.

valuable to use adsorption free energies calculated by DFT for describing the stages of heterogeneous catalysis [5,6]. The Wolkenstein's electronic approach based on weak and strong chemisorption of reaction intermediates was also applied to explain the volcano-shaped size dependence of reaction rate [7]. According to this approach, the position of the Fermi level is one of the main factors that determine the chemisorption strength of reagents on the catalyst surface and, consequently, the rate of the catalytic reaction. Using the example of oxide semiconductor systems (NiO, WO_3, Cr_2O_3, ZnO), it was shown how the rate of the catalytic reactions can be controlled by changing the position of the Fermi level at the crystal surface by introducing modifying impurities into the entire semiconductor volume [8,9]

One of the reasons for the limited use of Wolkenstein's theory in heterogeneous catalysis concerns the complexity in determining the energy levels of the surface states formed by adsorbates on the catalyst. However, its use is possible for oxides of transition metals (WO_3, TiO_2, ZrO_2, V_2O_5, Nb_2O_5) that exhibited a relation between the surface Fermi level of the solid and its activity through the surface acidity [10].

Zinc oxide is an n-type wide-band gap semiconductor that demonstrates the quantum confinement effect in a range of particle sizes less than 10 nm defined by a blue shift in the ultraviolet–visual (UV-Vis) absorption spectra [11]. The quantum confinement effect has been observed in various applications of ZnO nanoparticles, such as photocatalysts, varistors, sensors, solar cells, transparent electrodes, and electroluminescent devices [12–14].

In heterogeneous catalysis, zinc oxide is used as a support, an active component, a promoter, and a model system [15,16]. The high melting point of ZnO (1975 °C) promotes its application as a structural and textural modifier of multicomponent solid catalysts for organic synthesis, dehydration of hydrocarbons, and purification of technological and exhaust gases [17,18]. Zinc and its oxide do not exhibit high catalytic activity in the redox reactions due to the filled d-shell. The catalytic activity of zinc oxide in the oxidation reactions is associated with the presence of oxygen vacancies on its surface, which are centers of oxygen adsorption from the gas phase and at the same time active centers of reactions. The smaller the particle size, the greater the number of such centers on a catalyst surface. Using the X-ray photoelectron spectroscopy (XPS) technique, it was shown that the appearance of additional peaks in the photoelectron spectra of zinc oxide with a decrease in size of nanoparticles to less than 10 nm is due to the presence of oxygen vacancies on its surface [19,20]. We observed experimentally such a volcano-shaped size dependence of the surface-specific activity, i.e., the so-called turnover frequency (TOF), in CO oxidation over ZnO nanoparticles [21].

In the present study, we apply the Wolkenstein's electronic theory of catalysis to the CO oxidation reaction over zinc oxide nanoparticles in a narrow size range (4.0–4.6 nm) and compare the model with the experimental data on the size dependence of the reaction rate.

2. Results and Discussion

The ZnO/MgO samples with the different average diameters of ZnO nanoparticles in the narrow range of 4.0–4.6 nm were prepared by varying the conditions of the colloidal solution synthesis (reagent concentrations, aging temperature, and aging time). To eliminate the possible effects related to nanoparticle sintering, variations in active site distribution, and differences in metal loading, all ZnO/MgO samples were prepared with a constant ZnO content of 1 wt.%. This approach ensures that the total amount of ZnO and, consequently, the nominal density of active sites per gram of catalyst remain unchanged for all solids. Moreover, previous studies have shown that the applied preparation procedure does not induce significant changes in the textural properties of the MgO support, and the specific surface area remains essentially unaffected [21]. The particle diameter distribution

for ZnO/MgO solids was calculated assuming that ZnO nanoparticles are spherical and the optical absorption intensity (A) in diluted system is determined by the number of nanoparticles with a certain diameter [22]:

$$n(d) \propto -\frac{dA(d)/dd}{(1/6)\pi d^3} \quad (1)$$

where d is the particle diameter; $n(d)$ is the particle diameter distribution, and $n(d) = 0$ when $d \to \infty$; $A(d)$ is the optical absorption. The average diameter of ZnO nanoparticles was calculated as $<d> = \Sigma n(d_i)d_i/\Sigma n(d_i)$, where $n(d_i)$ is the number of particles with diameter d_i.

Typical UV-Vis DR spectra and the corresponding particle size distributions for ZnO/MgO solids with the different average diameters of ZnO nanoparticles are shown in Figure 1. It is worth noting that the ZnO particle size distribution calculated using Equation (1) is in good agreement with the distribution derived from the TEM analysis, as demonstrated in Ref. [21]. In contrast to Ref. [21], where the nanoparticle radius was used as the characteristic size parameter, in the present work, we report and analyze the data in terms of nanoparticle diameter.

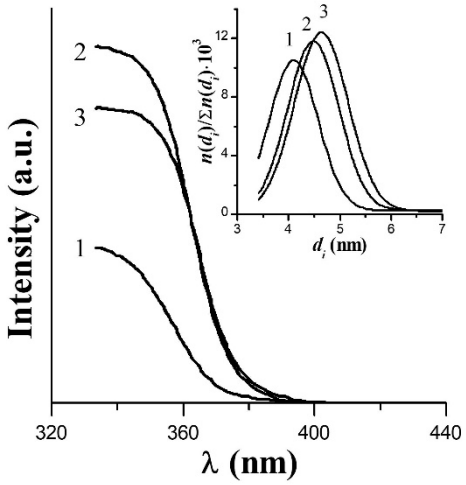


Figure 1. UV-Vis DR spectra and the particle size distribution for ZnO/MgO solids with the different average diameters of ZnO nanoparticles <*d*>: 1—4.1 nm; 2—4.4 nm; 3—4.5 nm. Conditions of the ZnO colloidal solutions preparation before their deposition over MgO powder: 1—[$Zn(CH_3COO)_2$] = 4.8 × 10^{-3} M; [NaOH] = 7.7 × 10^{-3} M; temperature for aging is 60 °C; aging time is 10 min; 2—[$Zn(CH_3COO)_2$] = 5.7 × 10^{-3} M; [NaOH] = 1.14 × 10^{-2} M; temperature for aging is 60 °C; aging time is 10 min; 3—[$Zn(CH_3COO)_2$] = 5.7 × 10^{-3} M; [NaOH] = 1.14 × 10^{-2} M; temperature for aging is 60 °C; aging time is 50 min. The ZnO content in the prepared samples amounted to ca. 1 wt.%.

The measurements revealed that essentially all of the quantum size effects of an increased band gap for ZnO nanoparticles occur by a shift in the conduction band edge due to the electron confinement. The position of the conduction band is raised when the particle diameter decreases from 4.6 to 4.0 nm, while the valence band is almost constant regardless of the particle size.

The size-dependent band gap (E_g, eV) for the spherical ZnO nanoparticles with diameter d (m) was defined from the analysis of the UV-Vis DR spectra using the effective mass model as a sum of three terms [23]:

$$E_g(d) = E_g^{bulk} + \frac{h^2}{2d^2}\left(\frac{1}{m_e^*} + \frac{1}{m_h^*}\right) - \frac{1.8e^2}{2\pi\varepsilon\varepsilon_0 d}, \quad (2)$$

where E_g^{bulk} is the bulk band gap (about 3.2 eV at room temperature for ZnO); h is the Planck's constant (6.626 × 10^{-34} Js); m_e^* and m_h^* are the effective masses for electron and

hole, respectively; for ZnO, $m_e^* = 0.26\ m_e$ and $m_h^* = 0.59\ m_e$; m_e is the free electron mass (9.11×10^{-31} kg); ε is the dielectric constant (8.5 for ZnO); ε_0 is the vacuum electric permittivity (8.854×10^{-12} $C^2N^{-1}m^{-2}$); e is the charge of a free electron (1.602×10^{-19} C). Expression (2) shows that the confinement energy increases the band gap, while the Coulomb interaction lowers the energy. The $1/d^2$ dependence is predominant in comparison with the $1/d$ scale; therefore, the confinement effect defines the size dependence of the band gap. It causes the band gap shift, when the band gap is larger for small particles.

The catalytic activity of the ZnO/MgO samples with an average particle diameter of 4.0–4.6 nm was evaluated for CO oxidation by O_2 in the temperature range of 200–500 °C and estimated as TOF. Figure 2 demonstrates the dependence of the band gap (left scale) and the CO oxidation rate, expressed as TOF at 320 °C (right scale), on the average diameter of ZnO nanoparticles in the ZnO/MgO solids. It shows that the band gap widens with decreasing nanoparticles size. For ZnO nanoparticles with a 4.6 nm diameter, the band gap difference is less than 0.2 eV compared to bulk ZnO (3.2 eV), and it increases up to 0.4 eV for the smallest particles (4.0 nm). The change in band gap is accompanied by a manifestation of volcano-shaped dependence of TOF on the average particle diameter of ZnO nanoparticles in solids. The ZnO/MgO solid containing ZnO nanoparticles of an average size of about 4.4 nm has maximum activity in CO oxidation. It should be noted that the catalysts obtained under different conditions but containing ZnO nanoparticles of the same size exhibit comparable activity in CO oxidation within the experimental error limit. Therefore, the volcano-shaped dependence of the ZnO/MgO solid activity on the band gap and average diameter of ZnO nanoparticles in the range of 4.0–4.6 nm may be attributed to the quantum confinement effect manifested by the electronic transition from the highest occupied molecular orbital (HOMO) to the lowest unoccupied molecular orbital (LUMO).

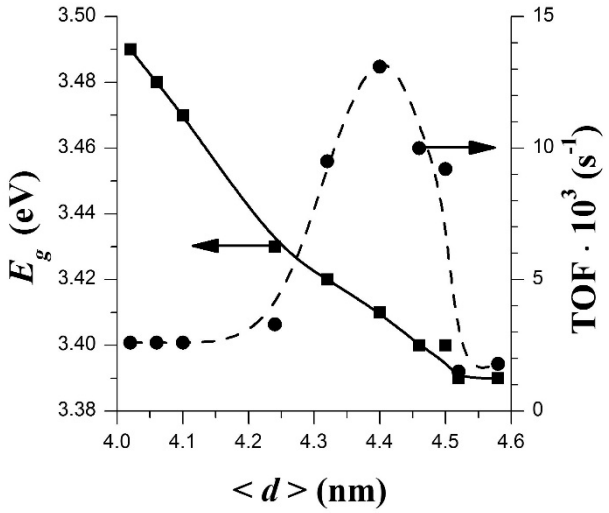


Figure 2. The dependence of the band gap (■, left scale, solid line) and the CO oxidation rate, expressed as TOF at 320 °C (●, right scale, dashed line), on the average diameter of ZnO nanoparticles in the ZnO/MgO solids.

In a non-generate semiconductor, the Fermi level is inside the band gap. The ZnO bulk semiconductor is considered as n-type because of the presence of intrinsic vacancy defects in the structure [15]. For the n-type ZnO, the Fermi level lies near the conduction band due to the presence of an excess of electrons that are located at an extra energy level [24]. Thus, we suppose that, by decreasing the size, the Fermi level mostly changes due to the quantum confinement of electrons:

$$E_F(d) = E_F^{bulk} - \frac{h^2}{2em_e^* d^2} \quad (3)$$

where E_F^{bulk} is the Fermi level of bulk ZnO solid. Because the Fermi level represents the average work performed to remove an electron from the material (work function), to calculate the change in Fermi level, we used the value of the work function for bulk ZnO equal to 5.3 eV [25].

The extension of the band gap in the ZnO/MgO solids is accompanied by a shift in the Fermi level position calculated by Equation (3) and presented in Figure 3.

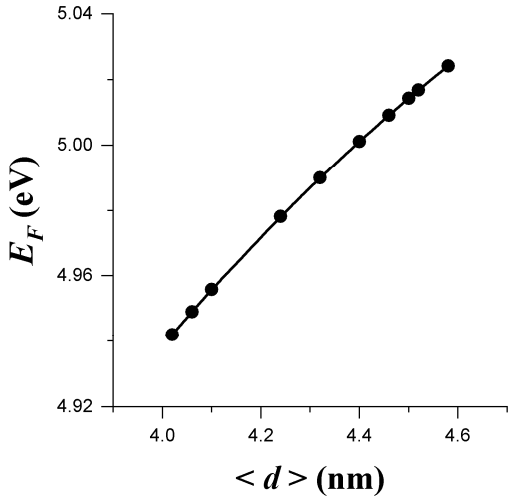


Figure 3. The dependence of the Fermi level position on the average diameter of ZnO nanoparticles in the ZnO/MgO solids.

The obtained volcano-shaped relation between the catalytic activity of the magnesia-supported ZnO nanoparticles and their size can be considered in the framework of Wolkenstein's electronic theory that establishes a correlation between the catalytic activity and the electrical conductivity of semiconductors since both are related to the Fermi level [8,9]. The experimentally proven factors influencing the position of the Fermi level and, accordingly, the activity of catalysts were doping, illumination, the external electric field, and the structural defects of a surface. Wolkenstein foresaw that the dispersion of a material can also be a factor affecting the position of the Fermi level and the associated adsorption and catalytic properties. The results of our work show, due to the quantum confinement effect that occurs in ZnO nanoparticles smaller than 10 nm, size is also a decisive factor controlling the position of the Fermi level and the activity of the ZnO/MgO catalyst with respect to the CO oxidation reaction.

According to Wolkenstein's theory, the heterogeneous catalytic reactions are divided into two classes based on the position of the Fermi level: reactions accelerated by electrons and their rate increases with an increase in the Fermi level (n-type acceptor reactions) and reactions accelerated by holes and their rate increases with a decrease in the Fermi level (p-type donor reactions). There are reactions whose mechanism includes both donor and acceptance stages. Wolkenstein considered a possible mechanism for such reactions using the example of CO oxidation on ZnO whose surface is completely covered with chemisorbed oxygen [8,9].

The Wolkenstein's mechanism is in good agreement with the Eley–Rideal scheme of CO oxidation on ZnO in an excess of oxygen [26,27] which is given below:

$$O_2 + 2Z \rightleftarrows 2ZO^0 \quad (1)$$

$$ZO^0 + \bar{e} \rightleftarrows ZO^- \quad (2)$$

$$ZO^- + CO \rightleftarrows ZCO_2^- \quad (3)$$

$$ZCO_2^- \rightleftarrows ZCO_2^0 + \bar{e} \quad (4)$$

$$ZCO_2^0 \rightarrow CO_2 + Z \quad (5)$$

In the above scheme of CO oxidation mechanism on ZnO, Z is the empty active site of the catalyst.

According to the proposed scheme, the mechanism of CO oxidation proceeds through dissociative adsorption of oxygen molecules onto the surface of the catalyst (1). Oxygen intermediates are activated by accepting electrons from the catalyst (2). In the ion-radical state, they react with CO molecules from the gas phase, and the ion-radicals of CO_2^- molecules are formed (3). CO_2^- intermediates are neutralized by donating electron to the catalyst (4), and then CO_2 desorbs from the surface (5). Thus, the mechanism of CO oxidation on ZnO includes two stages: an acceptor stage, when the electron is transferred from the catalyst to the reactant (O_2 and CO), and a donor stage, when the electron returns to the catalyst with the desorption of reaction product (CO_2). The extremal dependence of ZnO activity explains that the ratio of the rates of the acceptor and donor stages of the CO oxidation reaction depends on the position of the Fermi level on the surface of the ZnO nanoparticle.

The reaction rate of CO oxidation through the dissociative adsorption of oxygen molecules and interaction of adsorbed atomic oxygen with gas-phase CO molecules is defined in the following way after taking into account the dependence of the fractions of atomic oxygen and CO_2 as a function of the Fermi level [8]:

$$R = k_5 N^0_{CO_2} = \frac{k_3 k_5 P_{CO}}{k_3 P_{CO} s_O + s_O k_5 + \left[s_O + \sqrt{\frac{2k_{-1}}{k_1 P_{O_2}}}\right] k_{-3} e^{\frac{E^a_O - E^d_{CO_2}}{k_B T}} + (k_3 P_{CO} + k_{-3}) s_O e^{\frac{E_F - E^d_{CO_2}}{k_B T}} + k_5 \left[s_O + \sqrt{\frac{2k_{-1}}{k_1 P_{O_2}}}\right] e^{-\frac{E_F - E^a_O}{k_B T}}} \quad (4)$$

where $N^0_{CO_2}$ is the concentration of the adsorbed CO_2 in the neutral state corresponding to weak chemisorption; E_F is the Fermi level; E^a_O and $E^d_{CO_2}$ are the acceptor and donor energy levels of atomic oxygen and CO_2 on the catalyst surface, respectively; k_B is the Boltzmann constant; T is the temperature; P is the partial pressure of CO or O_2; s_O is the area of the catalyst surface occupied by one chemisorbed oxygen atom (the effective surface area of a single active site); k_1, k_3, and k_5 are the reaction rate constants of the appropriate stages (see the scheme above); k_{-1} and k_{-3} are the reverse rate constants of the appropriate stages. The substitution of Equation (3) into Equation (4) yields the following expression for the reaction rate as a function of the nanoparticle diameter (d):

$$R = \frac{1}{A + Be^{-\frac{D}{d^2}} + Ce^{\frac{D}{d^2}}} \quad (5)$$

where

$$A = \frac{s_O(k_3 P_{CO} + k_5) + k_{-3}\left(s_O + \sqrt{\frac{2k_{-1}}{k_1 P_{O_2}}}\right) e^{\frac{E^a_O - E^d_{CO_2}}{k_B T}}}{k_3 k_5 P_{CO}}$$

$$B = \frac{s_O(k_3 P_{CO} + k_{-3}) e^{\frac{E^{bulk}_F - E^d_{CO_2}}{k_B T}}}{k_3 k_5 P_{CO}}$$

$$C = \frac{\left(s_O + \sqrt{\frac{2k_{-1}}{k_1 P_{O_2}}}\right) e^{\frac{E^a_O - E^{bulk}_F}{k_B T}}}{k_3 P_{CO}}$$

$$D = \frac{h^2}{2k_B T} \frac{1}{m^*_e}$$

All four parameters (A, B, C, D) must be available for evaluation of the reaction rate using Equation (5), which is not always the case. However, Equations (4) and (5) allow one to make a qualitative analysis of the relation between the reaction rate and the energy of the Fermi level and the size of nanoparticles of the catalyst (Figure 4). By solving the differential equation $\frac{dR}{dd} = 0$, we can find the optimal size of ZnO nanoparticle diameter at which the reaction rate is maximum:

$$d_{opt} = \sqrt{\frac{2D}{\ln(C/B)}} \quad (6)$$

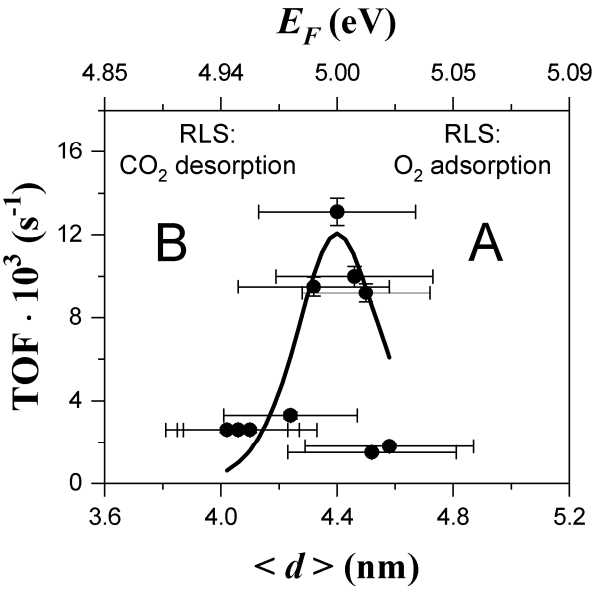


Figure 4. The dependence of the turnover frequency (TOF) in CO oxidation on the average diameter and the Fermi level of ZnO nanoparticles obtained experimentally (points) and through calculations (curve) with an indication of the rate-limiting step (RLS) in the corresponding region: A—O_2 adsorption; B—CO_2 desorption. The following parameters of Equation (5) were selected for calculated curve: A = 3.07 × 10^{-2} s, C = 2.46 × 10^7 s, B = 2.77 × 10^{-11} s, D = 400 nm^2. Reaction conditions: 2 vol.% CO, 20 vol.% O_2, He as a balance gas, flow rate = 100 $cm^3 min^{-1}$, P = 1 atm, T = 320 °C.

The application of Equations (4) and (5) to the CO oxidation over ZnO nanoparticles indicates that the value of the Fermi level decreases with a decrease in size of ZnO nanoparticles from 4.6 nm to 4.4 nm while the reaction rate increases, reaching a maximum value at 4.4 nm (Figure 4, region A). In region A, the donor stage of electron transfer to the catalyst proceeds easily, but the acceptor stage of electron transfer from the catalyst is slower. Therefore, the rate-limiting stage is O_2 adsorption onto the catalyst surface. As the Fermi level rises with the decrease in size, the adsorption of the oxygen improves; as a result, the reaction rate increases and reaches its peak. With a further decrease in the ZnO nanoparticle size to smaller than 4.4 nm, the Fermi level decreases, and the reaction rate begins to decrease (Figure 4, region B). Thus, in region B, the acceptor stage of electron transfer from the catalyst is facilitated, but the donor stage is hampered, i.e., the reaction rate is determined by CO_2 desorption from the catalyst surface. The observed "volcano" trend occurs within a narrow particle size window of approximately 0.4 nm, while the standard deviation of the ZnO particle size is about the same value. Despite this, the peak in catalytic activity remains well defined, indicating that the sharp increase in TOF is a genuine effect rather than an artifact of size variability or measurement uncertainty. Horizontal error bars in Figure 4 represent the particle size standard deviation, and vertical bars reflect the reproducibility of TOF measurements, demonstrating the statistical reliability of the

observed trend. This confirms that the catalytic activity is highly sensitive to particle size within this narrow range.

The idea of the relationship between the electron state in a solid and its catalytic properties was first expressed by L.V. Pisarzhevskii [28]. Later, these ideas were developed in Wolkenstein's works, who proposed the principles of a collective approach to explaining the catalytic properties of materials having a semiconductor nature [8,9]. Despite its popularity, the electronic theory has been criticized for not always finding experimental evidence. This was evidently due to the experimental possibilities of time, which did not always allow the accurate measurement of Fermi levels in semiconductors. An important consequence of the electronic theory is the prediction of the role of size factors on the catalytic properties of semiconductors. In one of his latest works, Wolkenstein noted that the high dispersity of a semiconductor material can have the same effect as impurities on the catalytic properties [9]. In particular, it has been shown that, by changing the thickness of the oxide semiconductor film on the copper surface, it was possible to control the position of the Fermi level and, accordingly, the adsorption capacity, activity, and selectivity of copper [8,29]. Wolkenstein did not attribute this result to a manifestation of the quantum size effect, but pointed out that quantum mechanics gave chemistry physical content and thus revealed the physical nature of chemical forces [8]. The relationship between the electronic properties and the thickness of the oxide film in VO_x, MoO_x, WO_x, and NbO_x deposited on alumina, zirconia, and magnesia was demonstrated in [30]. For these oxides, which are two-dimensional film domains, the TOF value in the reactions of ethane and propane dehydrogenation increased monotonically with a decrease in the edge energy of the absorption band, which was determined from the blue shift in the electron diffuse reflectance spectra. Also, the unusually high activity and selectivity of nanosized gold is associated with the manifestation of quantum size effects [31]. The bell-shaped dependence of the CO oxidation rate on the size of gold nanoparticles can be explained by a change in the electronic properties of two-layer gold nanoclusters stabilized on the support surface [32]. The Fermi level shift towards lower values was detected for gold nanoparticles in the Au/TiO_2 nanocomposite: 0.02, 0.04, and 0.06 eV for Au nanoparticles with a diameter of 8, 5, and 3 nm, respectively. This effect was caused by the unusual property of Au nanoparticles to undergo quantized charging [33]. It was shown that a promising way to control the catalytic activity of gold nanoparticles is tailoring the Fermi level of support [34]. The correlations of the gold nanoparticles' catalytic activity with the Fermi level of the support via electronic metal–support interactions were found in the oxidation reactions of CO and benzyl alcohol. For 4 mol % Cu/ZnO synthesized by four different methods, the influence of the preparation method on the position of the Fermi level and the selectivity of the synthesis gas conversion to higher alcohols was demonstrated. It was shown that the introduction of isolated Cu^{2+} atoms into the ZnO structure contributes to a decrease in the Fermi level, an increase in the carbon chain, and the corresponding increase in the proportion of C_2-C_6 alcohols to 69.9% [35].

Our results provide experimental evidence supporting Wolkenstein's approaches to explaining the catalytic properties of semiconductor oxides. Specifically, we obtained the confirmation of the volcano-shaped dependence of the CO oxidation rate on ZnO, as predicted by Wolkenstein, based on the position of the Fermi level. Furthermore, we successfully demonstrated the validity of Wolkenstein's prediction regarding the relationship between the dispersion of semiconductor material ZnO and its electronic characteristics. Our research revealed that the availability of electron energy states in the catalyst for participating in redox reactions strongly depends on its size, primarily due to the quantum confinement effect. Through the measurements of UV-Vis diffuse reflectance spectra, we examined the size-dependent band gap of ZnO nanoparticles within a narrow range of

4.0–4.6 nm. Our findings indicated that, as the particle size decreases, the Fermi level decreases due to the quantum confinement of free electrons, leading to changes in the conduction band edge. By leveraging the size dependence of the Fermi level and Wolkenstein's electronic theory of catalysis, we established the existence of an optimal size for nanoparticles catalyzing a two-stage chemical reaction (acceptor and donor stages). At this specific size of ZnO nanoparticles (about 4.4 nm in diameter), we observed that the reaction rate reaches its maximum value.

3. Experiments

3.1. Synthesis

ZnO/MgO solids with different controllable diameters of ZnO nanoparticles were prepared by a two-step method including the synthesis of the ZnO nanoparticle colloidal solutions from zinc acetate and sodium hydroxide in isopropanol followed by their deposition over MgO powder. The detailed synthesis method was described in [21,36]. The content of ZnO in prepared samples was determined by titrimetric analysis and amounted to ca. 1 wt.%.

3.2. Measurements and Characterization

The average size and size distribution of the ZnO nanoparticles in ZnO/MgO samples were obtained from their UV-Vis diffuse reflectance (DR) spectra using the spectrophotometer "Specord M-40" (Zeiss, Jena, Germany). MgO was used as a reference white standard for recording UV-Vis DR spectra. The zinc oxide dilution with magnesia minimizes the distortion of the diffuse reflectance spectra of prepared solids due to a regular (surface) reflection, which always the observation of even the finest grain sizes of crystallites [37]. As a result of several repeated UV-Vis DR spectra for each sample, the precision between the calculated values of the ZnO nanoparticle average diameter was $\pm$0.02 nm.

The prepared ZnO/MgO samples were tested in the CO oxidation reaction by oxygen using the flow method with the test gas mixture of 2 vol.% CO, 20 vol.% O_2, and He as a balance gas, at a flow rate of 100 cm^3min^{-1} under atmospheric pressure. All experiments were performed at a temperature of 320 °C. The reaction components and products (CO, O_2, CO_2) were analyzed at the reactor outlet by a gas chromatograph NEOCHROM (Zaporizhia, Ukraine). Repeating the catalytic experiment several times for each ZnO/MgO solid gave the reproducibility of a set of measurements, with a precision of $\pm$5%.

The CO oxidation rate was calculated in the kinetic reaction mode when CO conversion of less than 20% occurred for most of the prepared catalysts [38]. Under such conditions, the CO oxidation rate depends weakly on the concentrations of CO and O_2, the influence of reverse reaction is minimized, and the observable rate of CO oxidation is the closest to the true value. The value of TOF (s^{-1}) in the CO oxidation reaction for prepared catalysts was calculated as the number of CO molecules reacting per surface-centered ZnO molecules (active sites) in unit time. The number of active sites was obtained using the average diameter of the near-spherical ZnO nanoparticle.

4. Conclusions

An important consequence of Wolkenstein's electron theory of catalysis on semiconductors is the potential to exert control over the adsorption and catalytic properties of finely dispersed semiconductor materials through the regulation of the Fermi level. Within the context of the Eley–Rideal's CO oxidation mechanism on ZnO nanoparticles, we have demonstrated that an increase in the ZnO nanoparticles diameter in the region below 10 nm leads to a corresponding elevation in the Fermi level. This elevation, in turn, results in an accelerated acceptor stage and a decelerated donor stage involving free electrons in

the interaction with atomic oxygen, carbon monoxide, and carbon dioxide on the catalyst surface. Such opposite behavior between the donor and acceptor stages generates an inverted relationship in their rates, leading to a volcano-shaped dependence on the size of the ZnO nanoparticles. Consequently, an optimal catalyst particle size exists where the reaction rate reaches its maximum value.

Author Contributions: Conceptualization, G.K. and P.S.; Methodology, G.K. and N.T.; Validation, G.K. and O.D.; Formal Analysis, G.K., O.D. and P.S.; Investigation, G.K. and O.D.; Resources, O.D. and G.K.; Data Curation, G.K. and O.D.; Writing—Original Draft, G.K., N.T. and O.D.; Writing—Review and Editing, G.K., N.T., O.D. and P.S.; Visualization, G.K. and O.D.; Supervision, P.S.; Project Administration, N.T. and P.S.; Funding Acquisition, N.T. and P.S. All authors have read and agreed to the published version of the manuscript.

Funding: This research received no external funding.

Data Availability Statement: The data presented in this study are available in the article.

Conflicts of Interest: The authors declare no conflicts of interest.

References

1. Sabatier, P. Hydrogénations et déshydrogénations par catalyse. *Ber. Dtsch. Chem. Ges.* **1911**, *44*, 1984–2001. [CrossRef]
2. Strizhak, P.E. Nanosize effects in heterogeneous catalysis. *Theor. Exp. Chem.* **2013**, *49*, 2–21. [CrossRef]
3. Murzin, D.Y. On the optimum catalyst for structure sensitive heterogeneous catalytic reactions. *Reac. Kinet. Mech. Cat.* **2020**, *131*, 5–17. [CrossRef]
4. Murzin, D.Y. Kinetics of two-step catalytic sequence on nanoclusters with limited cluster occupancy. *J. Chem. Eng.* **2022**, *450*, 138178. [CrossRef]
5. Nørskov, J.K.; Bligaard, T.; Hvolbæk, B.; Abild-Pedersen, F.; Chorkendorff, I.; Christensen, C.H. The nature of the active site in heterogeneous metal catalysis. *Chem. Soc. Rev.* **2008**, *37*, 2163–2171. [CrossRef] [PubMed]
6. Nørskov, J.K.; Bligaard, T.; Logadottir, A.; Kitchin, J.R.; Chen, J.G.; Pandelov, S.; Stimming, U. Trends in the Exchange Current for Hydrogen Evolution. *J. Electrochem. Soc.* **2005**, *152*, J23–J26. [CrossRef]
7. Turaeva, N.; Krueger, H. Wolkenstein's Model of Size Effects in CO Oxidation by Gold Nanoparticles. *Catalysts* **2020**, *10*, 288. [CrossRef]
8. Wolkenstein, T. The Electron Theory of Catalysis on Semiconductors. *Adv. Catal.* **1960**, *12*, 189–264.
9. Wolkenstein, T. *Electronic Processes on Semiconductor Surfaces during Chemisorption*; Springer: New York, NY, USA, 1991.
10. Nandakumar, N.K.; Seebauer, E.G. Relating Catalytic Activity of d^0 Semiconducting Metal Oxides to the Fermi Level Position. *J. Phys. Chem. C* **2014**, *118*, 6873–6881. [CrossRef]
11. Repp, S.; Erdem, E. Controlling the exciton energy of zinc oxide (ZnO) quantum dots by changing the confinement conditions. *Spectrochim. Acta A Mol. Biomol. Spectrosc.* **2016**, *152*, 637–644. [CrossRef]
12. Oprea, O.; Andronescu, E.; Ficai, D.; Ficai, A.; Oktar, F.N.; Yetmez, M. ZnO Applications and Challenges. *Curr. Org. Chem.* **2014**, *18*, 192–203. [CrossRef]
13. Janotti, A.; Van de Walle, C.G. Fundamentals of zinc oxide as a semiconductor. *Rep. Prog. Phys.* **2009**, *72*, 126501. [CrossRef]
14. Park, Y.; Yoo, R.; Park, S.R.; Lee, J.H.; Jung, H.; Lee, H.S.; Lee, W. Highly sensitive and selective isoprene sensing performance of ZnO quantum dots for a breath analyzer. *Sens. Actuators B Chem.* **2019**, *290*, 258–266. [CrossRef]
15. Wöll, C. The chemistry and physics of zinc oxide surfaces. *Prog. Surf. Sci.* **2007**, *82*, 55–120. [CrossRef]
16. Liu, Y.; Guan, Y.; Li, C.; Lian, J.; Gan, G.; Lim, E.; Kooli, F. Effect of ZnO additives and acid treatment on catalytic performance of Pt/WO3/ZrO2 for n-C7 hydroisomerization. *J. Catal.* **2006**, *244*, 17–23. [CrossRef]
17. Chen, C.; Hu, Z.; Ren, J.; Zhang, S.M.; Wang, Z.; Yuan, Z.Y. ZnO supported on high-silica HZSM-5 as efficient catalysts for direct dehydrogenation of propane to propylene. *Mol. Catal.* **2019**, *476*, 110508. [CrossRef]
18. Sun, Y.; Chen, L.; Bao, Y.; Zhang, Y.; Wang, J.; Fu, M.; Wu, J.; Ye, D. The Applications of Morphology Controlled ZnO in Catalysis. *Catalysts* **2016**, *6*, 188. [CrossRef]
19. Tay, Y.Y.; Li, S.; Sun, C.Q.; Chen, P. Size dependence of Zn binding energy in nanocrystalline ZnO. *Appl. Phys. Lett.* **2006**, *88*, 173118. [CrossRef]
20. Janotti, A.; Van de Walle, C.G. Oxygen vacancies in ZnO. *Appl. Phys. Lett.* **2005**, *87*, 122102. [CrossRef]
21. Didenko, O.Z.; Kosmambetova, G.R.; Strizhak, P.E. Size effect in CO oxidation over magnesia-supported ZnO nanoparticles. *J. Mol. Catal. A Chem.* **2011**, *335*, 14–23. [CrossRef]

22. Pesika, N.S.; Stebe, K.J.; Searson, P.C. Relationship between Absorbance Spectra and Particle Size Distributions for Quantum-Sized Nanocrystals. *J. Phys. Chem. B.* **2003**, *107*, 10412–10415. [CrossRef]
23. Hu, Z.; Oskam, G.; Searson, P.C. Influence of solvent on the growth of ZnO nanoparticles. *J. Colloid. Interface Sci.* **2003**, *263*, 454–460. [CrossRef] [PubMed]
24. Ohtani, B. Photocatalysis by inorganic solid materials: Revisiting its definition, concepts, and experimental procedures. *Adv. Inorg. Chem.* **2011**, *63*, 395–430. [CrossRef]
25. Jacobi, K.; Zwicker, G.; Gutmann, A. Work function, electron affinity and band bending of zinc oxide surfaces. *Surf. Sci.* **1984**, *141*, 109–125. [CrossRef]
26. Boreskov, G.K. *Heterogeneous Catalysis*; Nova Sciense Publishers Inc.: New York, NY, USA, 2003.
27. Ma, D.; Wang, Q.; Li, T.; Tang, Z.; Yang, G.; He, C.; Lu, Z. CO catalytic oxidation on Al-doped graphene-like ZnO monolayer sheets: A first-principles study. *J. Mater. Chem. C* **2015**, *3*, 9964–9972. [CrossRef]
28. Pisarzhevskiy, L. *Electron in Chemistry*; Publishing House of the Academy of Sciences of the Ukrainian SSR: Kiev, Ukraine, 1956. (In Russian)
29. Roginsky, S. *Adsorption and Catalysis on Heterogeneous Surfaces*; Publisher of Academy of Sciences of USSR: Moscow, Russia, 1948.
30. Macht, J.; Iglesia, E. Structure and function of oxide nanostructures: Catalytic consequences of size and composition. *Phys. Chem. Chem. Phys.* **2008**, *10*, 5331–5343. [CrossRef]
31. Chen, J.; Cai, Y.; Yan, Z.; Goodman, D.W. On the origin of the unique properties of supported Au nanoparticles. *J. Am. Chem. Soc.* **2006**, *128*, 6341–6346. [CrossRef]
32. Haruta, M. Size- and support-dependency in the catalysis of gold. *Catal. Today* **1997**, *36*, 153–166. [CrossRef]
33. Subramanian, V.; Wolf, E.E.; Kamat, P.V. Catalysis with TiO_2/gold nanocomposites. Effect of metal particle size on the Fermi level equilibration. *J. Am. Chem. Soc.* **2004**, *126*, 4943–4950. [CrossRef]
34. Shinichi, N.; Teranishi, M.; Aoki, R.; Tada, H. Fermi level control of gold nanoparticle by the support: Activation of the catalysis for selective aerobic oxidation of alcohols. *J. Phys. Chem. C* **2016**, *120*, 12440–12445. [CrossRef]
35. Li, F.; Jia, P.; Zhang, Q.; Liu, Y.; Vinokurov, V.A.; Huang, W. Electronic control of catalytic activity of ZnO for higher alcohols synthesis via tailoring Fermi level. *Fuel Process. Technol.* **2023**, *241*, 107600. [CrossRef]
36. Strizhak, P.E.; Didenko, O.Z.; Kosmambetova, G.R. Synthesis and characterization of ZnO/MgO solids prepared by deposition of preformed colloidal ZnO nanoparticles. *Mater. Lett.* **2008**, *62*, 4094–4096. [CrossRef]
37. Kortüm, G.; Braun, W.; Herzog, G. Principles and Techniques of Diffuse-Reflectance Spectroscopy. *Angew. Chem. Int. Ed.* **1963**, *2*, 333–341. [CrossRef]
38. Zhdanov, V.P.; Kasemo, B. Simulations of the reaction kinetics on nanometer supported catalyst particles. *Surf. Sci. Rep.* **2000**, *39*, 25–104. [CrossRef]

Disclaimer/Publisher's Note: The statements, opinions and data contained in all publications are solely those of the individual author(s) and contributor(s) and not of MDPI and/or the editor(s). MDPI and/or the editor(s) disclaim responsibility for any injury to people or property resulting from any ideas, methods, instructions or products referred to in the content.